THE HEATING FIELD IN AN ASYMMETRIC HURRICANE—— PART II: RESULTS OF COMPUTATIONS

T. N. Krishnamurti and *Sheng Jian* (盛 剑)

Department of Meteorology, Florida State University, U.S.A.

Received October 20, 1984.

ABSTRACT

This is the second part of a paper on the distribution of heating fields in a hurricane. The first part dealt with the mathematical framework. The second part, i. e. the present paper deals with numerical calculations for an actual hurricane.

The following sequence of calculations has been performed after the analysis and tabulation of an initial field of the tangential velocity $U(r, \theta, p)$: (1) the radial equation of motion is used to determine the geopotential heights; (2) the hydrostatic equation is used to determine the temperature field; (3) the tangential equation and the mass continuity equation are combined to obtain an omega equation whose solution determines the vertical velocity; (4) the radial velocity is next determined from the mass continuity equation; and (5) the heating function is finally determined from the first law of thermodynamics.

The results of this study show an asymmetric banded structure (eye wall and rainband) of the vertical motion field as well as the heating field; these show close resemblence to observations. An analysis of the non-linearities of the asymmetric momentum distribution is shown to be crucial in the analysis of the hurricane heat sources.

I. INTRODUCTION

In the first part[1] of this paper we presented a scale analysis for the low-order description of a hurricane (or a typhoon). This is an inverse problem where the heat sources and sinks are calculated for a given distribution of the angular momentum. A local cylindrical coordinate (r, θ, p) is used to formulate this problem. An expansion parameter e, which is a ratio of the convergence above the boundary layer to that in the boundary layer, describes a low-order system in a gradient wind balance along the radial direction. The system permits full asymmetry in the azimuthal direction about the storm axis.

The results of a sequence of inverse calculations starting from the observed tangential velocity in a hurricane are presented in this paper. The sequence consists of solving for the vertical and radial velocity, the geopotential height and the thermal fields and finally the diabatic heating that maintains the entire system. The problem is similar in approach to that proposed in Krishnamurti (1961, 1962)[2,3]. Formal solutions are carried out to completion here and they are more revealing on the nature of the boundary layer, the asymmetric heating and the banded vertical motion fields. The scale analysis, furthermore, renders itself towards the construction of higher-order closed systems, which may be used to address limitations posed by the low-order solutions shown here.

II. SOLUTIONS OF EQUATIONS

1. *The Equation for the Vertical Velocity* ω'

For a prescribed tangential velocity U', the momentum and the mass continuity equation may be combined to eliminate V' and we obtain an equation for the vertical velocity ω'

$$\frac{\partial\omega'}{\partial p'}+a'\frac{\partial\omega'}{\partial r'}+\frac{\omega'}{r'}\frac{\partial(a'r')}{\partial r'}+\frac{1}{r'}\frac{\partial(b'r')}{\partial r'}+c'=0, \tag{1}$$

where $a'=-\dfrac{\partial U'/\partial p'}{\zeta_a'}$,

$$b'=\frac{1}{\zeta_a}\left\{-U'\frac{\partial U'}{\partial\lambda'}+\frac{\partial}{\partial r'}\left[\gamma'\left(\frac{\partial U'}{\partial r'}+\frac{U'}{r'}\right)\right]+\frac{\partial}{\partial p'}\left(K'\frac{\partial U'}{\partial p'}\right)\right\},$$

$$c'=\frac{\partial U'}{\partial\lambda'}.$$

A solution of Eq. (1) can be obtained by either the method of characteristics[2], or by simple numerical schemes[4,5]. A knowledge of ω' on top of the boundary layer is required to solve this problem.

2. *Boundary Layer and Boundary Conditions*

Ideally perhaps formal solution of scaled equations of a boundary layer should be matched with solutions of Eq. (1). Alternatively one could express the boundary layer convergence as a function of the curl of the wind stress on top of the boundary layer by assigning arbitrary values for the drag coefficient C_D. In this preliminary investigation we shall take a very simple and crude approach to define the boundary layer convergence. Based on the theory of the scale parameters λ_0 and R we shall set

$$\left.\frac{\partial\omega}{\partial p}\right|_{\text{Boundary Layer}}=\frac{\lambda_0}{R}\left.\frac{\partial\omega}{\partial p}\right|_{\text{Above boundary layer}}. \tag{2}$$

According to this scale analysis, relation (2) is only true to an order of magnitude.

A solution of the convergence field may be obtained for Eq. (1) above the boundary layer. We find that this field is in general banded with regions of convergence and divergence. The region of convergence agrees well with the region of radar bands[3]. In this earlier study no formal boundary layer was incorporated and the calculations were performed with unscaled non-dimensional equations. Because of the good agreement between the convergence, computed from data above the boundary layer, and the radar bands we suggest that the boundary layer convergence must be strongly correlated to the convergence above the boundary layer. This view is along the lines of the so-called hot-tower hypothesis of Riehl and Malkus[6]. If air parcels are carried up from the surface boundary layer with large magnitudes of the heat content to great heights with little lateral mixing, the large convergence field in the boundary layer should agree with the location of cloud bands. Hence we parameterize the boundary layer convergence according to Eq. (2).

3. *Asymmetries of the Momentum Distribution*

In order to portray the relation between the tangential velocity U and the banded convergence determined by the inviscid asymmetric terms, i. e.

$$\left.\frac{\partial \omega}{\partial p}\right|_{A} = -\frac{\partial}{\partial r}\frac{U}{\zeta_a}\frac{\partial U}{r\partial\theta} - \frac{\partial U}{r\partial\theta},$$

we shall illustrate the following fields at the 900 hPa surface for Hurricane Helene of 1958: (Data for U is obtained in the manner shown in Ref. [3])

1) U,

2) ζ_a,

3) $\partial V/r\partial\theta$,

4) $U\dfrac{\partial U}{r\partial\theta}$,

5) $\dfrac{U}{\zeta_a}\dfrac{\partial U}{r\partial\theta}$,

6) $-\dfrac{\partial}{\partial r}\dfrac{U}{\zeta_a}\dfrac{\partial U}{r\partial\theta} - \dfrac{\partial U}{r\partial\theta}$.

The tangential velocity U (knots) shows the familiar asymmetry in the speed field (Fig. 1). The corresponding field of absolute vorticity (Fig. 2) ζ_a (10^{-4} sec^{-1}) shows a similar asymmetry, the largest values of ζ_a are close to 40 units, in the region of interest, $r<150$ km, flow is cyclonic at all points, maximum vorticity is found at a distance of about 25 km from the storm center, while the largest tangential velocity is at a distance of 30 km from the storm center. Fig. 3 shows the field of $\dfrac{\partial U}{r\partial\theta}$ in non-dimensional units. Along the line $\dfrac{\partial U}{r\partial\theta}=0$, θ is not constant because of large asymmetries in the tangential velocity field. For a symmetric storm moving with a constant speed the field of $\dfrac{\partial U}{r\partial\theta}$ would be symmetric about a line $\theta=$const. Fig. 4 shows the field of $U\dfrac{\partial U}{r\partial\theta}$ in non-dimensional units. This field is similar to that of $\dfrac{\partial U}{r\partial\theta}$, the asymmetric nature of the tangential velocity field is evident from the large negative center of 700 units compared to a positive center of 400 units, and the zero line is obviously the same for the fields of $\dfrac{\partial U}{r\partial\theta}$ and $\dfrac{U\partial U}{r\partial\theta}$. The field of $\dfrac{U}{\zeta_a}\dfrac{\partial U}{r\partial\theta}$ (Fig. 5) (in non-dimensional units) is particularly interesting, largest values are close to 125 units and are located 40 to 50 km from the storm center, values greater than 75 units are found at distances of 100 km from storm center because of smaller

values of the absolute vorticity. This is a significant result because the radial gradient of this quantity is large at different distances from the storm center and contributes to the convergence of the velocity field. A careful examination of this figure thus reveals the banded nature of the radial gradients of the isolines. This is the complex form of the relationship of the momentum distribution of the mesoscale flows and the banded convergence.

Fig. 6 shows the field of convergence $\left.\frac{\partial \omega}{\partial p}\right|_{A} = -\frac{\partial}{\partial r}\frac{U}{\zeta_a}\frac{\partial U}{r\partial\theta} - \frac{\partial U}{r\partial\theta}$. Near the storm center $r<40$ km the main contribution comes from both terms, but for $r>40$ km the essential contribution is from the first term. The field is banded, showing both convergence and divergence fields resemble the pattern of radar echoes (Fig. 7). Figs. 1 and 6 portray the relation between U and $\partial\omega/\partial p|_A$. The only conclusion that can be drawn from these figures is that a mesoscale (larger than 10 km) banded convergence field is a consequence of mass and momentum balance when the latter contains asymmetries. The tangential motion is a smoothed input in this analysis and does not contain wavelengths smaller than 10 km. To maintain this smoothed large-scale momentum distribution in steady state a large scale (>10 km) banded convergence is required.

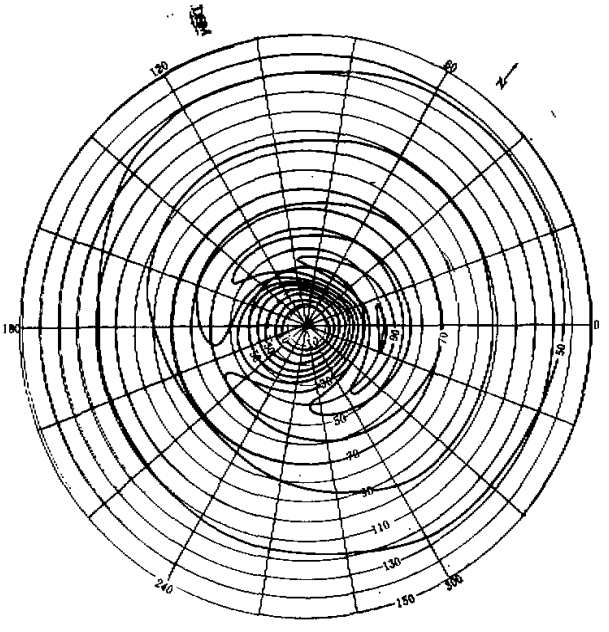

Fig. 1. Tangential velocity, knots, at the 900 hPa surface in Hurricane Helene (Sept. 26, 1958).
Radial distance of polar coordinates is marked in km and angular distance in degrees. Letter N represents north and DSM the direction of storm motion.

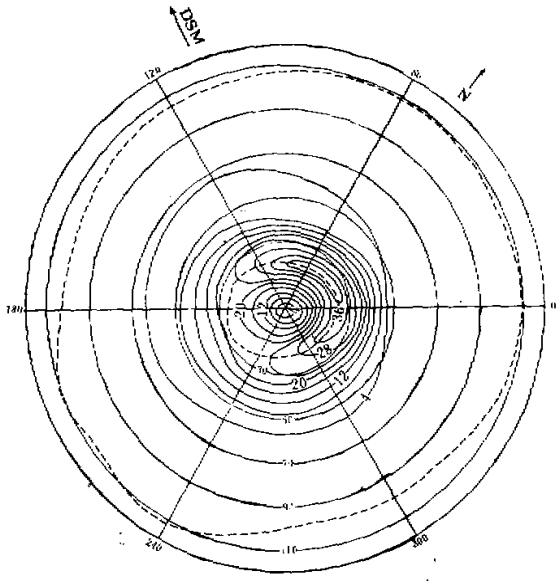

Fig. 2. As in Fig. 1, except for absolute vorticity, in 10^{-5} sec^{-1}.

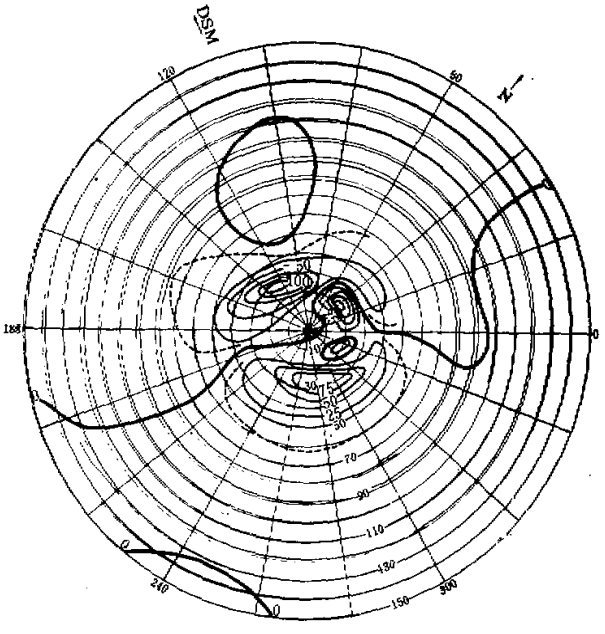

Fig. 3. As in Fig. 1, except for the field of $\frac{\partial U}{r\partial\theta}$, non-dimensional units.

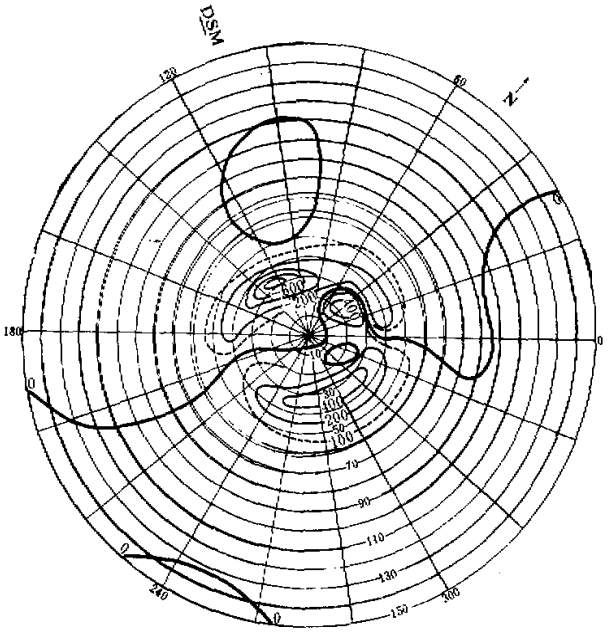

Fig. 4. As in Fig. 1, except for the field of $U-\frac{\partial U}{r\partial\theta}$, non-mendisional units.

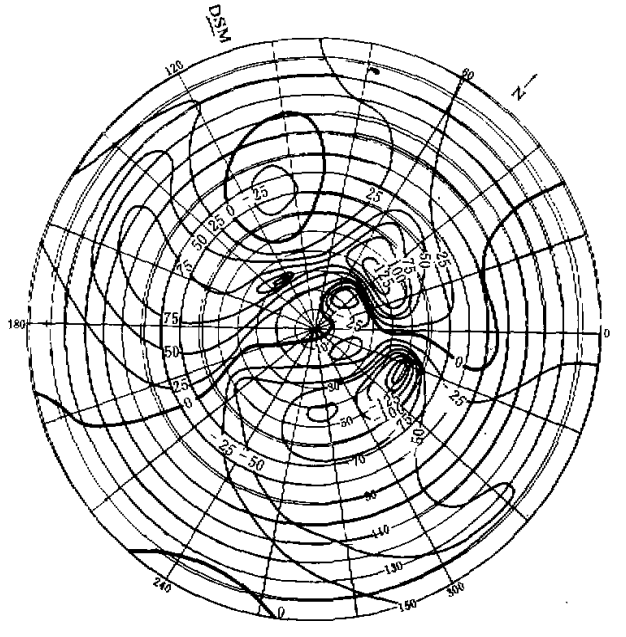

Fig. 5. As in Fig. 1, except for the field of $\frac{U}{\zeta_a}\frac{\partial U}{r\partial\theta}$, non-dimensional units.

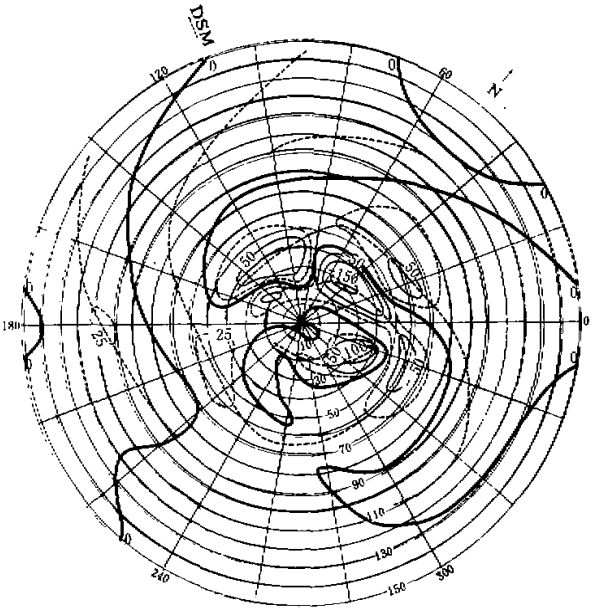

Fig. 6. As in Fig. 1, except for the field of $-\frac{\partial}{\partial r}\frac{U\partial U}{\zeta_a \partial \theta}-\frac{\partial U}{r\partial \theta}$, non-dimensional units.

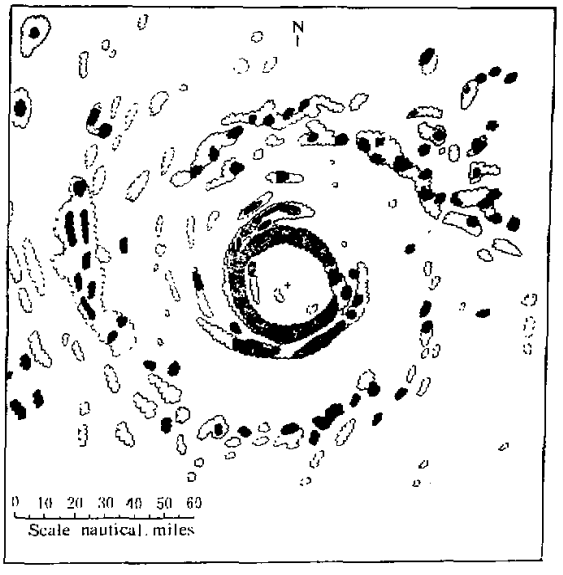

Fig. 7. A radar composite echo chart for Hurricane Helene, September 26, 1958. Dark and light echoes are marked in different shades. The information is based on aircraft reconnaissance flight with a 2 cm radar.

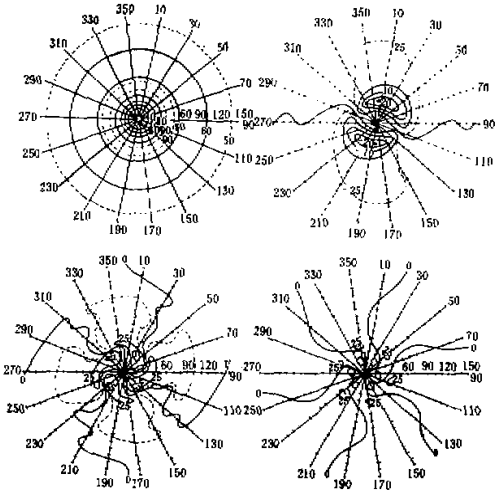

Fig. 8. Harmonic analysis of the 810 hPa tangential velocity distribution in Hurricane Helene, September 26, 1958 (knots). The first, second, third and fourth harmonics are respectively displayed in top left, top right, bottom left and bottom right. Radial distance is marked in km and the tangential distance in degrees.

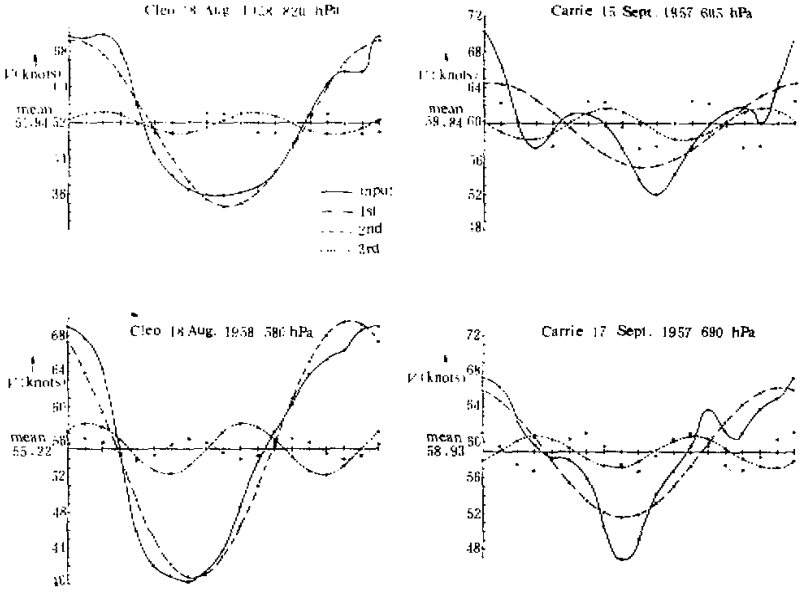

Fig. 9. Harmonic analysis of the tangential velocity field for Hurricane Cleo of 1958 and Carrie of 1957 at different pressure levels. The ordinate indicates wind speed in knots. The abscissa is a line along the circumference of a circle at an approximate radius of maximum wind. The points along the abscissa are taken in a counter-clockwise sense starting from the maximum tangential wind.

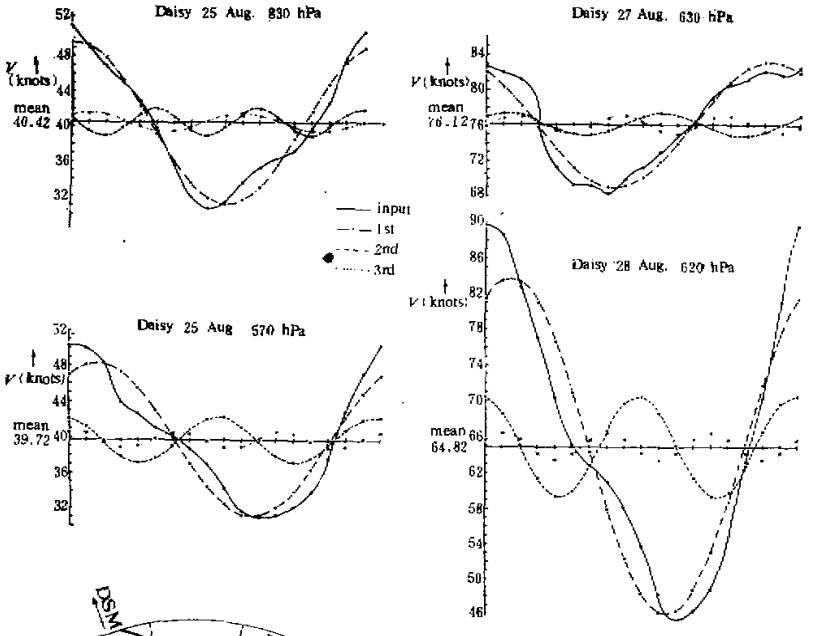

Fig. 10. As in Fig. 9, except for Hurricane Daisy of 1958.

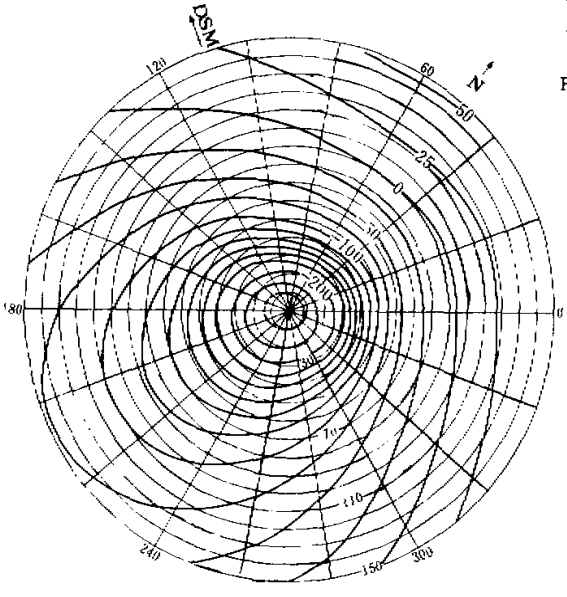

Fig. 11. Computed D-value at the 900 hPa surface in meters for Hurricane Helene, 26 Sept. 1958. The mean D-value is assumed zero at $r=150$ km. Letter N represents north and DSM the direction of storm motion.

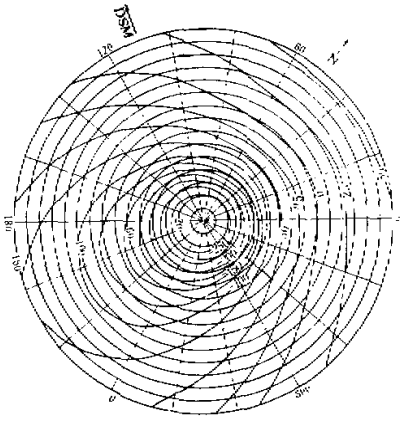

Fig. 12. As in Fig. 11, except for the 700 hPa surface.

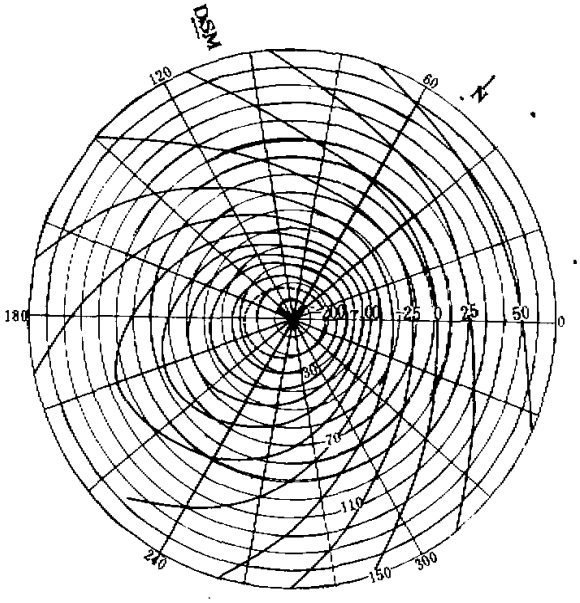

Fig. 13. As in Fig. 11, except for the 500 hPa surface.

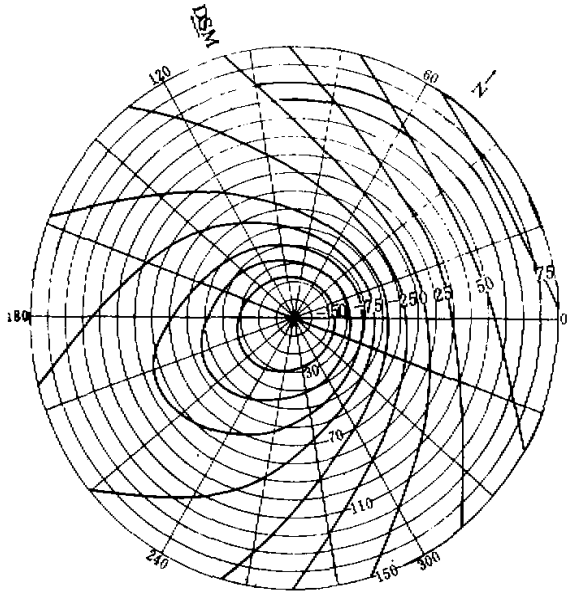

Fig. 14. As in Fig. 11, except for the 300 hPa surface.

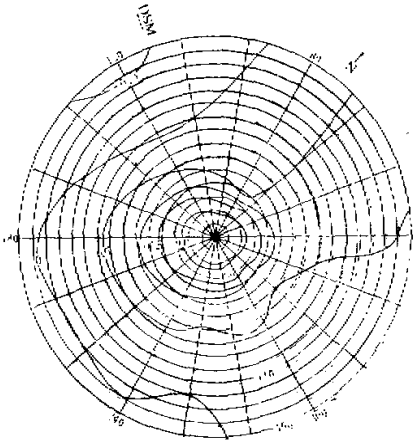

Fig. 15. Computed temperature anomaly at the 800 hPa surface, in °C, in Hurriane Helene. The mean temperature anoma'y is assumed zero at $r=150$ km.

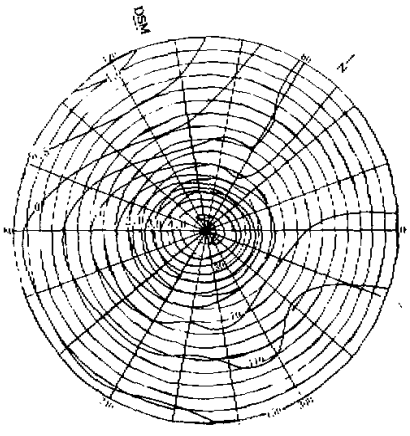

Fig. 16. As in Fig. 15, except for the 600 hPa surface.

We shall next examine the phase and amplitude of the asymmetries of the momentum distribution in hurricanes. An analysis similar to zonal harmonic analysis of 500 hPa heights in general circulation studies can be carried out about the storm axis to decompose the tangential velocity field into its harmonics at different radii. The results for the storm Helene of 1958, 810 hPa, are presented in Fig. 8. Of interest are the amplitudes in the first, second and third harmonics. The first harmonic has the largest amplitude over 20 knots, the second and third harmonics have amplitudes about 7 and 4 knots respectively. The speed of motion of the storm was considerably less, about 9 knots at this time. These asymmetries of the momentum distribution may be a consequence of complex interactions of a boundary layer flows and environmental flows with a symmetric vortex. Alternatively perhaps a re-examination of the notion of a symmetric model is in order.

There was a tendency for the maxima of the tangential velocity to shift downwind where the higher harmonics 2 and 3 were added to the first harmonic. This feature was found in several storms of the 1958 season that were examined (Figs. 9 and 10). The similarity in the phase shift of the second and third harmonics in relation to the first in several storms suggests that the first, second and third harmonics are standing modes in a reference frame moving with the storm. Figs. 9 and 10 portray the harmonic analysis of the wind field for several storms of the 1958 season. The abscissa in all these figures is a line taken along the circumference of a circle of maximum wind speed. The ordinate represents wind speed in knots. The study thus confirms our notion that the second and third harmonics can have considerable amplitude, over 7 knots in some cases. The maxima of all the harmonics

tend to appear close to that of the first harmonic, suggesting that they are anchored modes in a moving frame. The amplitudes of fourth and higher harmonics were generally smaller than 2 knots which is close to the limiting resolution of the Doppler winds.

Both low level (810 hPa) and high level (280 hPa) flights show considerable asymmetries. We might thus expect considerable amplitudes in the second and third harmonics in boundary layer flows. Flight at levels near the first kilometer above the sea level would be of considerable value for studying the asymmetries. Intuitively we should expect a similar picture in the boundary layer. Boundary layer convergence is partially determined by the advective terms of the vorticity equation where such asymmetries would be important. Hitherto most formulations[7,8], and several others, have only considered the effect of the curl of the wind stress in the vorticity equation for estimating the boundary layer convergence. These formulations describe a simple Ekman-type flow in the lowest kilometer; a modified Ekman problem with most of the terms retained in the vorticity equation would give an entirely different picture.

4. *The D-Value and the Temperature Fields*

The name D-value refers to an anomaly of the geopotential height from a standard atmosphere. D-values were computed at 300, 500, 700, and the 900 hPa surfaces (Figs. 11, 12, 13, and 14), and the temperature anomalies at the 400, 600, and 800 hPa surfaces (Figs. 15, 16 and 17). The calculations of the D-values are carried out in two steps: (i) Assuming $D=0$ at the outer region of the calculation, i. e. at $r=150$ km, a numerical integration is carried out to obtain the D-values for $r=0$ along different radial arms.

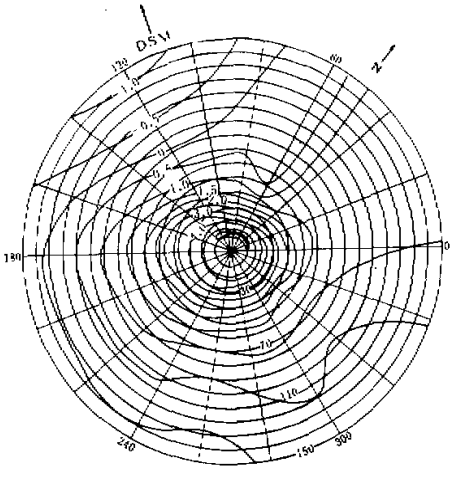

Fig. 17. As in Fig. 15, except for the 400 hPa surface.

(ii) These differing values at $r=0$ are then averaged and a numerical integration is carried out for $r>0$. The resulting D-values possess a vanishing mean at $r=150$ km, and a unique value at the center. The range of D-values at the 300 hPa surface are somewhat smaller than that at the 900 hPa surface as is to be expected. A comparison of the computed

D-values with the observed values from Colon's studies[9] are shown here in Fig. 18. The two results are in fair agreement at all levels if we assume that the D-values are identical at $r=150$ m, the outer radius of the calculations. The computed D-value at the center does not measure as intense a storm as the observed D-values suggest. The magnitude of the discrepancy is a few hundred feet and can be explained by incorporating higher-order terms, which would measure the gradient wind departures.

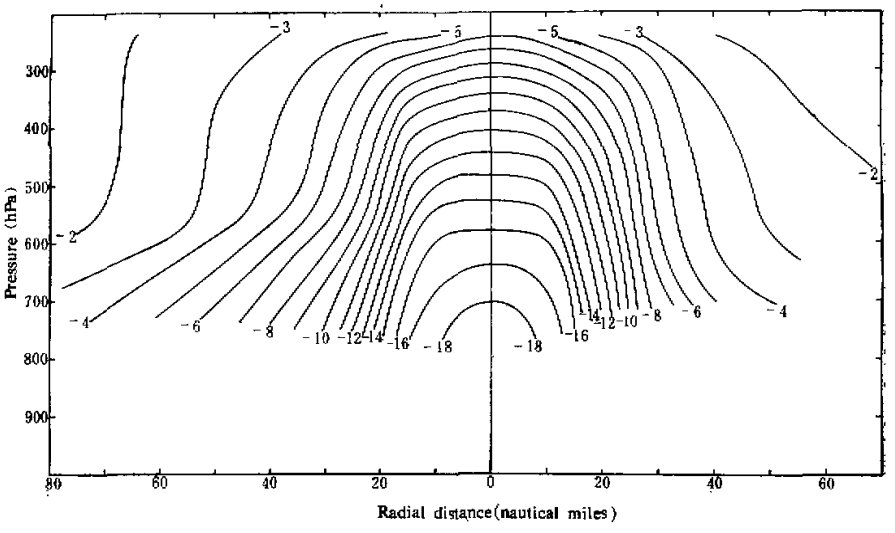

Fig. 18. A cross setion of the D-values in hundreds of feet in Hurricane Helene from left to right with respect to storm motion (After Colon, 1964).

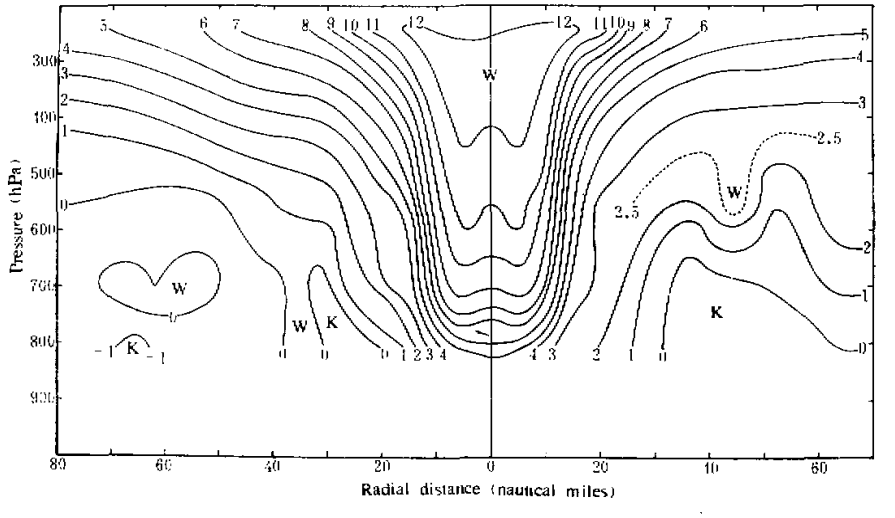

Fig. 19. As in Fig. 18, except for the temperature anomaly (°C).

Temperature anomalies are evaluated from the vertical gradients of the D-values. The warm core is quite symmetric about the storm center. The intensity of the warm core may be measured by the largest temperature differences between the storm center and the outer region near $r=150$ km. The magnitude of this difference is about 3°C at the 800 hPa surface and about 6°C at the 600 and 400 hPa surfaces. A vertical cross section of the temperature (Fig. 19) is taken from a study by Colon[9]; it shows an analysis of measured temperatures in the storm from three levels of flight data. Our computed temperatures show a less intense warm core than Colon's observation. This discrepancy could partially be explained by noting that the computed temperature anomalies assume a zero mean anomaly at $r=150$ km while those of Colon's observation show a temperature departure from a mean atmosphere of over 3°C. The computations give vertical averages over distances of around 200 hPa. In general, our results are thus in good agreement with those of Colon's.

The temperature distributions show a region in the far right front quadrants where the horizontal temperature gradients are very small, and are only 1 to 1.5°C warmer than the standard atmosphere. This is a region where the vertical wind shears are very small, and the temperature distribution is not clear, the results, however, are fairly reliable. The inner storm area $r<150$ km contains a strongly baroclinic region with horizontal temperature gradients as large as 1°C per 10 km and a barotropic region with temperature gradients less than 0.1°C per 10 km. This barotropic region contains the most widespread severe weather. A possible explanation for this might lie in vertical mixing in convective clouds where the large-scale vertical wind shears are rendered small. It would be of interest to examine these aspects of the temperature distribution in other storms in further detail.

5. *Vertical Motion and the Heating Field*

The results of calculation at the 700 hPa surface will be presented here. Eq (1) is integrated between 900 and 700 hPa surfaces with the assumption that the characteristic lines are vertical[3]. Boundary layer was assumed to be 100 hPa deep between the 1000 and 900 hPa surfaces. The non-dimensional coefficients ν' and K' are order of unity, they were made to vary in the r, θ space arbitrarily as a function of the non-dimensional velocity U'. This was primarily an outcome of a number of numerical experiments that were made on a trial and error basis; the choice $\nu'=K'=1$ was found to give unrealisitic results for $r<r_m$. Attempts to make ν' and K' proportional to ζ_a' gave too large rising motions near $r<r_m$. Finally it was decided to use,

$$\nu'=0.1\ U'$$
$$K'=0.1\ U'.$$

U' varies from 0.1 to 6, and hence ν' and K' vary from 0.01 to 1. It is not surprising that these non-dimensional quantities are not of order unity everywhere, because a characteristic velocity $V_0=10$ m/s generally represents velocities between 0 and 60 m/s.

The distribution of ω (Fig. 20), at the 700 hPa surface shows bands of rising and sinking motion. The largest rising motion is about -0.4 hPa/sec (≈ 4 m/s) and the largest sinking motion also about 0.4 hPa/sec. The horizontal distributions appear very realistic. A graph from left to right with respect to storm motion shown in Fig. 21 portrays the distribution of vertical motions above the boundary layer and at the 700 hPa surface. The calculated ω distributions display strong centers of rising and sinking motions in regions which could be designated as the wall cloud region and the eye. The diameter of the central sinking region is around 40 km, very close to that of the radar eye in Fig. 7. This distribution of

ω is similar to the equivalent black body temperature distributions produced from the analogue traces of high resolution infrared radiometric probes of Nimbus satellite over Hurricane Gladys (18 Sept. 1964 0422 U.T.) (Fig. 22). This figure was obtained from the files of NASA.

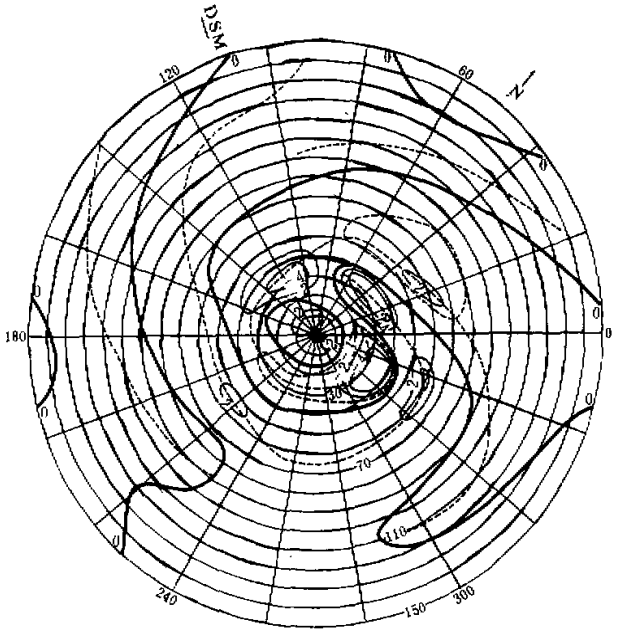

Fig. 20. Vertical motion at the 700 hPa surface in Hurricane Helene, in non-dimensional units.
The approximate conversion to dimensional units is: 1 unit$\approx 10^{-1}$ hPa sec≈ -1 m/s. Radial distance scale is marked in km and tangential scale in degrees. Letter N represnents north and DSM the direction of storm motion.

In this first experiment we have arbitrarily selected $\varepsilon = 0.1$, i. e. convergence in the boundary layer is 10 times that just above the boundary layer. Since there are regions of net divergence above the boundary layer, this results in strong region of divergence in the boundary layer. And as a consequence we have strong regions of sinking motion above the boundary layer. The geometry of sinking and rising motions (Fig. 20) compares very well with the position of clear and cloudy regions of Fig. 7.

In order to justify the validity of such magnitudes of vertical motions, calculations of heating function H were made from Eq. (46) in Part I[1] of this paper. The procedure is similar to that reported in Ref. [2]. Fig. 23 shows the distribution of diabatic heating (or cooling) required to maintain the system in steady state. As expected the results were very reasonable from moist parcel ascent considerations in regions of strong rising motions. However the regions of strong sinking motions are too intense and, to balance the adiabatic warming in these regions, a net cooling is required.

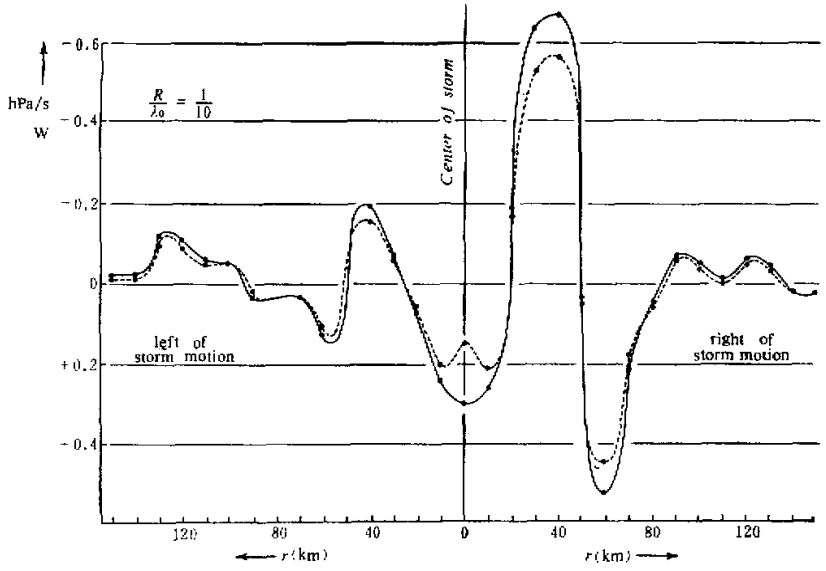

Fig. 21. Distribution of vertical motion at the top of the boundary layer (dashed lines), and at the 700 hPa surface (solid lines) from left to right of storm through the center of the storm.

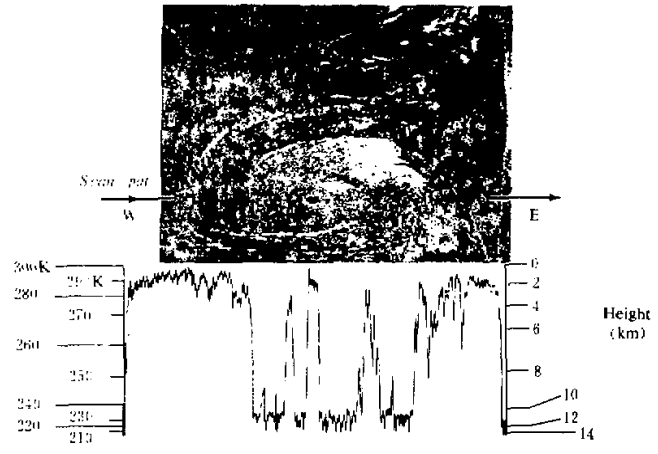

Fig. 22. An analogue trace of the equivalent black body temperature made by the High Resolution Infrared Radiometer in Hurricane Gladys by the Nimbus I satellite.

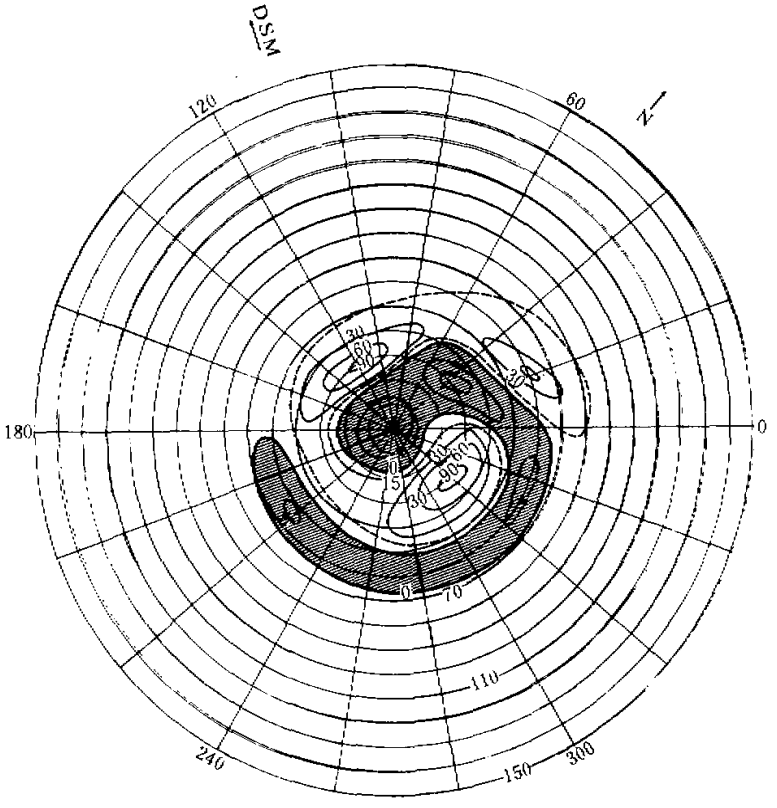

Fig. 23. Distribution of diabatic heating, required to maintain the observed momentum distribution in steady state, in Hurrciane Helene. Units 10^{-4} cal/(gm sec). Shaded region denotes cooling. Radial distane scale is marked in km and tangential scale is in degrees. Letter N represents north and DSM the direction of storm motion.

The discrepancy reported here is not serious because a reformulation of the boundary layer equations can indeed be made to either prevent regions of boundary layer divergence or permit small magnitudes such that no net cooling would be required for a steady state balance.

An alternate choice would have been to set

$$\left(\frac{\partial \omega}{\partial p}\right)_{\mathrm{I}} = \varepsilon \left(\frac{\partial \omega}{\partial p}\right)_{\mathrm{II}}, \text{ if } \left(\frac{\partial \omega}{\partial p}\right)_{\mathrm{II}} > 0. \tag{3}$$

And

$$\left(\frac{\partial \omega}{\partial p}\right)_{\mathrm{I}} = 0, \text{ if } \left(\frac{\partial \omega}{\partial p}\right)_{\mathrm{I}} < 0. \tag{4}$$

The corresponding solutions for Eq. (1) show a somewhat more realistic steady state picture.

Fig. 24 shows the geometry of mean boundary layer streamlines that permit regions of strong velocity divergence as well as convergence. The streamlines are drawn by solving Eq. (16) (Part I) for V', for given U' and $\frac{\partial \omega'}{\partial p'}$, the solution contains interesting convergence lines beneath the regions of strong rising motions of Fig. 20.

In order to obtain these streamlines in the planetary boundary layer we had to solve for the radial velocity utilizing Eq. (15) (Part I). The solution of the raidial velocity requires an outer boundary condition at $r = 150$ km. We have selected radial velocity $V = 3$ m s^{-1} at this outer boundary. These solutions of the flows (Fig. 24) in the planetary boundary layer are extremely interesting. They are dramatically consistent with the solutions of the other variables shown in this study.

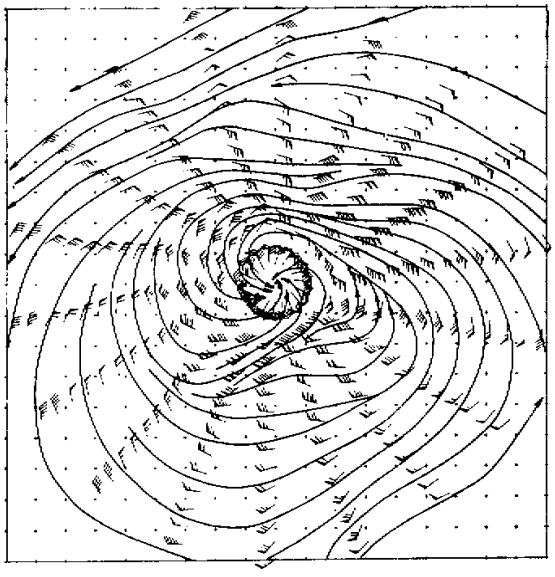

Fig. 24. Streamlines in the boundary layer of a hurricane computed from the model where regions of strong horizontal divergence are permitted. The horizontal radial scale is marked in km and the tangential scale in degrees.

III. CONCLUDING REMARKS

This is still a preliminary attempt towards a description of the three-dimensional mesoscale structure of a steady state hurricane. This attempt, like some of the previous investigations, has enabled a further understanding of the banded vertical motion field and its relations to the asymmetric momentum distribution. We feel that a complete three-

dimensional model that can satisfactorily describe the three-dimensional distribution of the dependent variables like U, V, ω, Z and T, both in the boundary layer and above, will be especially useful for studies of momentum, heat and energy balances. The precise manner by which large amounts of absolute angular momentum are brought into the inner storm region are still not properly understood. The steady state storm maintains a balance of angular momentum by a large transport from the outer regions of the storm while frictional torques are constantly transferring it to the earth. A better understanding of the boundary layer flows will enable a more complete picture of this aspect. The same description of the boundary layer flow would account for the sources of moisture and of diabatic heating over the ocean surface and it would be possible to see how the mesoscale ($>$ 10 km) vertical motions carry the heat up in the regions of strong rising motions and maintains a warm core. Subgrid-scale motion ($<$ 10 km) will appear in a parameterized form and it would be possible to study the effects of the cumulus scales in this manner.

In this paper we have shown that the banded structure of the vertical velocity in a hurricane is intimately related to the azimuthal asymmetries of the tangential velocity. Observations of the latter show that the major azimuthal variation of the tangential velocity is described by more than wave number one about the axis of rotations. That implies that the major asymmetry is not simple due to the translation of the storm. Higher harmonics usually result from the nonlinear advective terms which distort the translational asymmetry to produce higher harmonics as well as a shift in phase.

The azimuthal asymmetries of the momentum and the asymmetric heat sources and sinks (such as those in the eye wall and the spiral rainbands) coexist dynamically and one can not ascribe one to the cause of the other.

The magnitude of the net heating in the eye wall is of the order of 8×10^{-3}cal/(gm sec) which relates to about 500°C/day of warming; in the spiral bands the magnitude of heating is around 2×10^{-3} cal/(gm sec) which is about 120°C/day. Cooling in moist adiabatic ascent over regions where vertical motion is of the order of 1 m s^{-1} can be as large as 600°C/day. Thus the strong heating rates in the eye wall, stated here, are reasonable magnitudes.

To the lowest order the pressure and the temperature distributions are quasi-symmetric. A warm core of the order of 5°C warmer than the outer area is calculated by the proposed model. That is a slight underestimate compared to the observed structures reported by Hawkins and Rubsam[10]. We believe that this discrepency can be resolved by extending the calculations to higher order where the departure from the gradient wind laws would be included. That is a simple extension of the low-order system which can be obtained using the lower-order system as a first iteration for a successive correction and extension of the procedure.

This study has successfully reproduced the major asymmetries of the mature hurricane including those of the heat sources, thermal, pressure, vertical motion fields and the boundary layer flows.

Further extensions of this work including budgets of momentum, heat and kinetic energy for the low- and higher-order systems will be reported later.

The research reported here was supported by the National Science Foundation NSF grant No. ATM 83040809. The computations reported here were carried out at the NCAR CRAY. NCAR is sponsored

by the National Science Foundation. Mr. Sheng Jian would like to convey his appreciation to Nanjing University for permitting him to study at Florida State University.

Table 1 List of Symbols

r	radial coordinate, positive outward
θ	tangential coordinate, positive in the cyclonic sense
p	pressure, the vertical coordinate
U	tangential component of velocity
V	radial component of velocity
ω	vertical component of velocity
M	absolute angular momentum per unit mass
f_0, f	Coriolis parameter
ζ_a	absolute vorticity
$a=$	$-\frac{1}{\zeta_a}\frac{\partial U}{\partial p}$
$b=$	$-\frac{U}{\zeta_a}\left(\frac{\partial U}{r\partial\theta}\right)$
R	characteristic length scale in the radial direction
λ_0	characteristic tangential length scale
U'	non-dimensional tangential velocity
V'	non-dimensional radial velocity
Z	geopotential height
F_θ	frictional force per unit mass in the tangential direction
F_r	frictional force per unit mass in the radial direction
R_G	gas constant
H	non-adiabatic heating per unit mass
C_p	specific heat of air at constant pressure
H^*	scale height of the atmosphere
Ω	characteristic vertical velocity
g	acceleration of gravity
ν_r	radial eddy-momentum exchange coefficient
ν_λ	tangential eddy-momentum exchange coefficient
K	vertical eddy-momentum exchange coefficient
P	characteristic pressure
r_m	radius of the zone of maximum tangential velocity
I	symbol for the boundary layer
II	symbol for region above the boundary layer

REFERENCES

[1] Krishnamurti, T. N., *Adv. Atmos. Sci.*, **2**(1985), 3:402—413
[2] Krishnamurti, T. N., *Tellus*, **13**(1961), 171—180.
[3] Krishnamurti, T. N., *Tellus*, **14**(1962), 195—211.
[4] Barrientos, C. S., *J. Appl. Met.*, 1964, 685—692.
[5] Gilman, P. A., *Tellus*, **17**(1965), 274—302.
[6] Riehl, H. and Malkus J. S., *Tellus*, **13**(1961), 181—213.
[7] Yanai, M., *Reviews of Geophysics*, **2**(1964), 367—414.
[8] Ooyama, K., *A dynamical model for the study of tropical cyclone development*. Unpublished scientific report. Department of Meteorology and Oceanography, New York University.
[9] Colon, Jose, NHRL Report No. 72, 1964.
[10] Hawkins, H. F. and Rubsam D. T., *Mon. Wea. Rev.*, **97**(1968), 617—636.